EXPLAINING EXTREME EVENTS OF 2014

From A Climate Perspective

Special Supplement to the
Bulletin of the American Meteorological Society
Vol. 96, No. 12, December 2015

EXPLAINING EXTREME EVENTS OF 2014 FROM A CLIMATE PERSPECTIVE

Editors

Stephanie C. Herring, Martin P. Hoerling, James P. Kossin, Thomas C. Peterson, and Peter A. Stott

Special Supplement to the

Bulletin of the American Meteorological Society

Vol. 96, No. 12, December 2015

AMERICAN METEOROLOGICAL SOCIETY

Corresponding Editor:

Stephanie C. Herring, PhD
NOAA National Centers for Environmental Information
325 Broadway, E/CC23, Rm 1B-131
Boulder, CO 80305-3328
E-mail: stephanie.herring@noaa.gov

Cover credits:

Front: ©iStockphotos.com/coleong—Winter snow, Boston, Massachusetts, United States.

Back: ©iStockphotos.com/nathanphoto—Legget, California, United States – August 13, 2014: CAL FIRE helicopter surveys a part of the Lodge Fire, Mendocino County.

HOW TO CITE THIS DOCUMENT

Citing the complete report:

Herring, S. C., M. P. Hoerling, J. P. Kossin, T. C. Peterson, and P. A. Stott, Eds., 2015: Explaining Extreme Events of 2014 from a Climate Perspective. *Bull. Amer. Meteor. Soc.*, **96** (12), S1–S172.

Citing a section (example):

Yoon, J. H., S.-Y. S. Wang, R. R. Gillies, L. Hipps, B. Kravitz, and P. J. Rasch, 2015: Extreme fire season in California: A glimpse into the future? [in "Explaining Extremes of 2014 from a Climate Perspective"]. *Bull. Amer. Meteor. Soc.*, **96** (12), S5–S9.

EDITORIAL AND PRODUCTION TEAM

Riddle, Deborah B., Lead Graphics Production, NOAA/NESDIS National Centers for Environmental Information, Asheville, NC

Love-Brotak, S. Elizabeth, Graphics Support, NOAA/NESDIS National Centers for Environmental Information, Asheville, NC

Veasey, Sara W., Visual Communications Team Lead, NOAA/NESDIS National Centers for Environmental Information, Asheville, NC

Griffin, Jessicca, Graphics Support, Cooperative Institute for Climate and Satellites-NC, North Carolina State University, Asheville, NC

Maycock, Tom, Editorial Support, Cooperative Institute for Climate and Satellites-NC, North Carolina State University, Asheville, NC

Misch, Deborah J., Graphics Support, LMI Consulting, Inc., NOAA/NESDIS National Centers for Environmental Information, Asheville, NC

Osborne, Susan, Editorial Support, LMI Consulting, Inc., NOAA/NESDIS National Centers for Environmental Information, Asheville, NC

Schreck, Carl, Editorial Support, Cooperative Institute for Climate and Satellites-NC, North Carolina State University, and NOAA/NESDIS National Centers for Environmental Information, Asheville, NC

Sprain, Mara, Editorial Support, LAC Group, NOAA/NESDIS National Centers for Environmental Information, Asheville, NC

Young, Teresa, Graphics Support, STG, Inc., NOAA/NESDIS National Centers for Environmental Information, Asheville, NC

TABLE OF CONTENTS

ABSTRACT—Stephanie C. Herring, Martin P. Hoerling, James P. Kossin, Thomas C. Peterson, and Peter A. Stott

Understanding how long-term global change affects the intensity and likelihood of extreme weather events is a frontier science challenge. This fourth edition of explaining extreme events of the previous year (2014) from a climate perspective is the most extensive yet with 33 different research groups exploring the causes of 29 different events that occurred in 2014. A number of this year's studies indicate that human-caused climate change greatly increased the likelihood and intensity for extreme heat waves in 2014 over various regions. For other types of extreme events, such as droughts, heavy rains, and winter storms, a climate change influence was found in some instances and not in others. This year's report also included many different types of extreme events. The tropical cyclones that impacted Hawaii were made more likely due to human-caused climate change. Climate change also decreased the Antarctic sea ice extent in 2014 and increased the strength and likelihood of high sea surface temperatures in both the Atlantic and Pacific Oceans. For western U.S. wildfires, no link to the individual events in 2014 could be detected, but the overall probability of western U.S. wildfires has increased due to human impacts on the climate.

Challenges that attribution assessments face include the often limited observational record and inability of models to reproduce some extreme events well. In general, when attribution assessments fail to find anthropogenic signals this alone does not prove anthropogenic climate change did not influence the event. The failure to find a human fingerprint could be due to insufficient data or poor models and not the absence of anthropogenic effects.

This year researchers also considered other human-caused drivers of extreme events beyond the usual radiative drivers. For example, flooding in the Canadian prairies was found to be more likely because of human land-use changes that affect drainage mechanisms. Similarly, the Jakarta floods may have been compounded by land-use change via urban development and associated land subsidence. These types of mechanical factors re-emphasize the various pathways beyond climate change by which human activity can increase regional risk of extreme events.

18. THE DEADLY HIMALAYAN SNOWSTORM OF OCTOBER 2014: SYNOPTIC CONDITIONS AND ASSOCIATED TRENDS

S.-Y. Simon Wang, Boniface Fosu, Robert R. Gillies, and Pratibha M. Singh

The Himalayan snowstorm of October 2014 resulted from the unusual merger of a tropical cyclone with an upper trough, and their collective changes under climate warming have increased the odds for similar events.

The event. October 14, 2014, was a particularly dark day in the history of the Nepal Himalayas. An unanticipated blizzard initiated avalanches that killed 43 people, including 21 trekkers on the popular trekking routes of Mount Annapurna. The blizzard was connected with Cyclone Hudhud, a category 4 tropical cyclone (TC) that developed in the Bay of Bengal (BoB). After making landfall in eastern India, Hudhud proceeded northward towards Nepal. The synoptic evolution leading up to 14 October is illustrated in Fig. 18.1a, with daily 250-hPa winds and precipitation overlaid with Hudhud's location. During 12–13 October, a short-wave trough was moving eastward across the Himalayas. This trough deepened and subsequently collided with a weakening TC Hudhud on 13 October, forming a classic tropical-extratropical interaction (e.g., Kim et al. 2012; Riemer et al. 2014) that combined the abundant moisture supply associated with the remnants of Hudhud and the upstream upper-level trough, enhancing cross-mountain moisture fluxes. This interaction provided a dynamical mechanism for tropospheric ascent and caused stationarity of the weather systems, further compounding the orographic enhancement of precipitation in the Himalayas on October 14 (Fig. 18.1a).

Nepal is ranked the fourth most climate-vulnerable country in the world and it is prone to a wide variety of weather-related hazards that encompass droughts, floods, and landslides (Wang et al. 2013a; Gillies et al. 2013). Because Nepal has not yet established a warning system linked to weather forecasting, authorities did not issue an alert for the hazardous weather conditions that eventually led to the October 2014 disaster (Nair and Sharma 2014). However, BoB TCs of Hudhud's magnitude are not unprecedented, and neither are snowstorms in the Himalayas. Tropical-extratropical interactions in this area are rare but not unique, yet one associated with so much moisture is extraordinary. Hence, it is imperative to investigate the specific meteorological processes that trigger such extreme events, as well as the climatic processes that tend to enhance them, with a goal of improving future predictability.

Data and methodology. Two global reanalyses were used: the NCEP–NCAR Reanalysis (R1; Kalnay 1996) that covers the 1948–2014 period and the satellite-era NCEP–DoE Reanalysis II (R2; Kanamitsu et al. 2002) beginning in 1979. Tropical cyclone tracks were obtained from the Joint Typhoon Warning Center (JTWC) best track records (www.usno.navy.mil). For the depiction of the event precipitation in October 2014, we used the NOAA Climate Prediction Center (CPC) morphing technique (CMORPH) global precipitation analyses derived from low-orbiter satellite microwave observations (Joyce et al. 2004). For the purposes of attribution, we analyzed the Coupled Model Intercomparison Project (CMIP5) historical single-forcing experiments (Taylor et al. 2012) that were driven by (i) anthropogenic aerosol forcing only (AERO), (ii) anthropogenic greenhouse gas forcing only (GHG), and (iii) natural only, including solar and volcanic forcings (NAT)—these were initialized from long stable preindustrial (1850) control settings and simulated up to 2005. We adopted seven models as listed in Supplemental Table S18.1. In this paper, the season analyzed covers the two-month period from September 15 to November 15.

A few variables were derived from the reanalyses: (i) transient eddies associated with synoptic-scale dis-

AFFILIATIONS: Wang and Gillies—Utah Climate Center, and Department of Plants, Soils, and Climate, Utah State University, Logan, Utah; Fosu—Department of Plants, Soils, and Climate, Utah State University, Logan, Utah; Singh—Department of Hydrology and Meteorology, Kathmandu, Nepal, and Utah Climate Center, Utah State University, Logan, Utah

DOI: 10.1175/BAMS-D-15-00113.1

A supplement to this article is available online (10.1175/BAMS-D-15-00113.2)

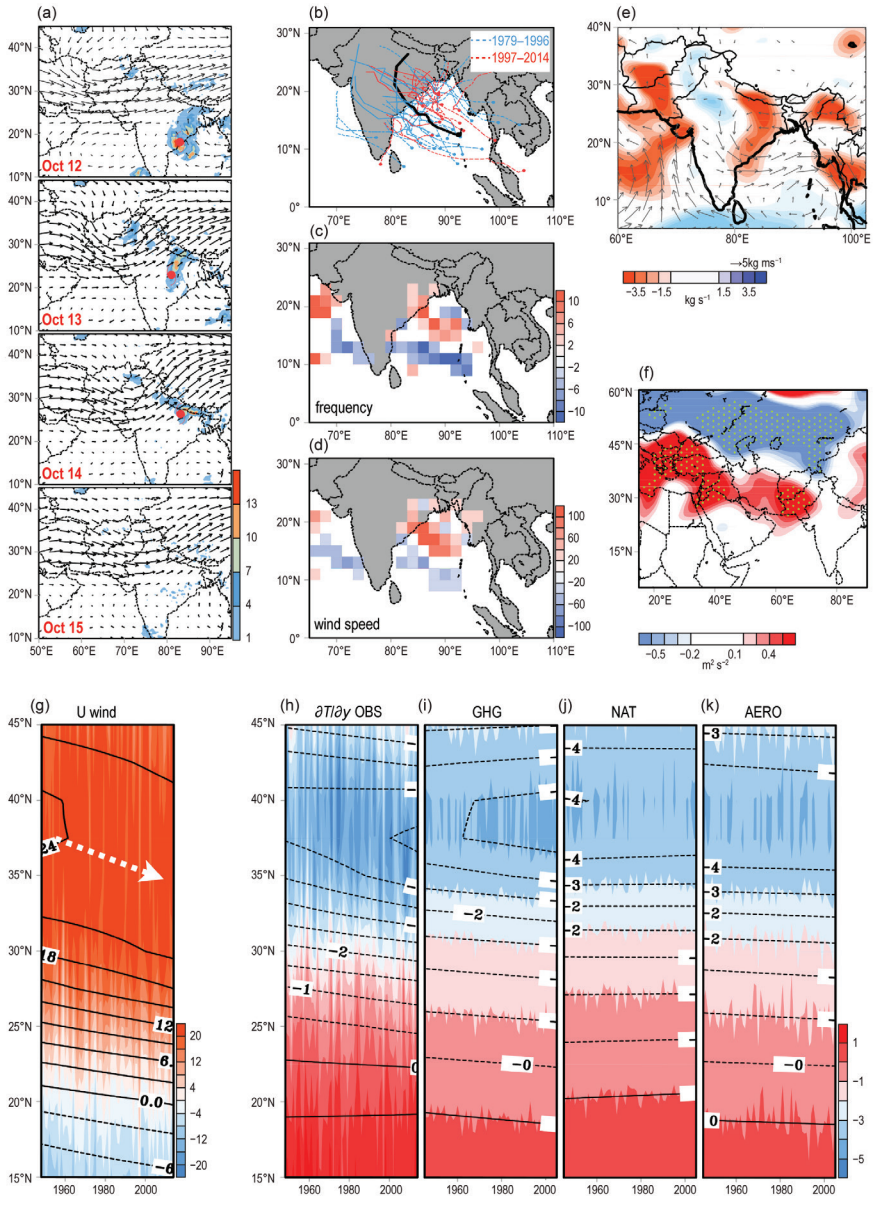

Fig. 18.1. (a) Daily evolution of the 250-hPa wind vectors and CMORPH precipitation (shadings) from 12–15 Oct 2014, overlaid with the location of TC Hudhud and its remnants as hurricane symbol. (b) Post-monsoon (Sep–Oct) TC tracks in the BoB over the period of 1979–2014, with the dotted lines showing the JTWC best tracks and solid lines depicting the residual lows defined through manual tracking. The track of TC Hudhud is shown by thick black line. (c),(d) Areal frequency differences of TC occurrences and maximum sustained wind speed, respectively, between the pre- and post-1997 periods after 1979; only values significant at $p < 0.05$ are plotted. (e) Total changes in Q (vectors), and mean $\nabla \cdot Q$ computed by the linear trend (slope) multiplied by the number of years from 1979 to 2014, using R2. (f) As in (e), but for the 250-hPa transient activity $\overline{v'}$ with the significant values ($p < 0.05$) represented by dots. (g) Latitude-time section of 250-hPa zonal wind (u) across 68°–78°E overlaid with the linear trends of u computed at each latitude over the 1948–2014 period (contours), using R1. The white arrow indicates southward shift of the jet. (h) As in (g), but for the 250-hPa meridional temperature gradient. (i)–(k) As in (h), but using the CMIP5 ensembles from the GHG, NAT, and AERO experiments (see text).

turbances that were computed from the variance of daily meridional winds at 250-hPa bandpass-filtered with 2–9 days, denoted as $\overline{v'}$ (e.g., Lau and Nash 1991). To depict TC remnants after making landfall, which are not included in the JTWC best tracks, we utilized 850-hPa streamline and vorticity analyses to track from each TC's last best-track position onwards until the center relative vorticity became smaller than 3×10^{-5} s^{-1}, following the tracking method of Chen et al. (2005) and using R2. We also projected the 6-h TC positions onto a 2 × 2 grid mesh, producing a gridded frequency (by count) and intensity (by maximum sustained wind speed) of BoB TCs. To understand the moisture budget, we computed the column water vapor flux (Q) by integrating up to 300 hPa and the moisture flux convergence ($\nabla \cdot Q$).

Results. a. Lower-level changes. Figure 18.1b shows the post-monsoon TC tracks since 1979, with TC Hudhud highlighted and the tracks before/after 1997 marked as blue/red. Unlike most BoB storms that dissipate quickly over land, Hudhud has been the only TC whose remnant ever reached as far north as the Himalayas. Moreover, post-1997 cyclones appear more concentrated in the northern BoB than before, suggesting an increase in the TC

threat to northern India. To verify this observation, we computed the areal frequency differences in TC occurrence (Fig. 18.1c) and maximum sustained wind speed (Fig. 18.1d) between the post- and pre-1997 periods. The result shows a significant increase in TC occurrence over the northern part of BoB, especially the stronger ones, but with a decrease over the southern bay. The impact of the changing TCs on the regional water budget is illustrated in Fig. 18.1e, which shows total changes in the seasonal-mean Q and $\nabla \cdot Q$ computed from their respective linear trend/slope multiplied by 36 years (1979–2014). A cyclonic anomaly of Q appears at BoB's northwestern shore accompanied by increased convergence of water vapor fluxes extended from the cyclonic center to Nepal, maximized along the foothill of the Nepalese Himalayas. The transient activity of moisture convergence (not shown) also is increased within the cyclonic anomaly of Q, and this corresponds with the change in TC tracks (Figs. 18.1b–d). Together, these results suggest an overall increase in the moisture transport associated with tropical disturbances in BoB, resulting in enhanced moisture pooling towards the Himalayas.

Previous research has noted an intensification in BoB TCs that supports our results. Recent studies (Wang et al. 2013b; Sahoo and Bhaskaran 2015) found that post-monsoon TCs have tended to grow more intense even though their number has decreased, and such intensification was a response to increased sea surface temperature (SST). Moreover, because the sustained increase in the Indian Ocean SST is linked to anthropogenic global warming (Rao et al. 2012), the observed intensification of post-monsoon BoB TCs is expected to continue in the future (Balaguru et al. 2014; Sarthi et al. 2015).

b. Upper-level changes. To examine whether and how the upper-level circulations conducive to short waves similar to the October 2014 case have changed, we examined the linear trend of the synoptic transient activity ($\overline{v}'$) at 250 hPa, which is shown in Fig. 18.1f. There is a universal increase in $\overline{v}'$ all the way from northern India to the Mediterranean Sea. Given the prevailing westerly flow, this band of increased $\overline{v}'$ implies a shift of the storm track diverting more and/or stronger short waves towards Nepal. This notion was validated from the latitude-time section of the 250-hPa zonal winds (u) across 68°E and 78°E, which is upstream of Nepal; this is shown in Fig. 18.1g from 1948 onwards using the R1 data. A southward migration of the jet is discernable, and this is further illustrated by the linear trend of u computed at each latitude (in y-axis) over the 1948–2014 period (in x-axis). Based on the contours around 30°N, the southward migration of the jet stream was estimated to be around 300 km since 1948, and this explains the increased $\overline{v}'$ in the southern flank of the jet stream.

So what affected the South Asian jet? To answer this question, we further analyzed the change in the meridional temperature gradients ($\partial T/\partial y$) at 250 hPa. Figure 18.1h depicts a clear equatorward shift in ($\partial T/\partial y$) which appears to have accelerated after 1990, corresponding to the zonal wind shift. This result suggests that the tropospheric warming that prevailed after the 1980s has modulated the jet maintenance related to thermal wind balance. To understand the role of external climate forcing in such a change, we derived ($\partial T/\partial y$) from the CMIP5 ensembles of GHG, NAT, and AERO-forcing experiments; these are shown in Figs. 18.1i–k. By visual comparison, the equatorward shift of ($\partial T/\partial y$) results primarily from GHG, which depicts a gradual equatorward migration (south of 35°N) with an expansion of the jet core (between 35°N and 40°N). The NAT forcing produced a slight poleward shift of ($\partial T/\partial y$), opposite to the observation. A possible secondary cause comes from AERO producing a southward shift that only occurred after 1990. This AERO-induced shift in the jet stream maintenance is likely linked to the recent increase in anthropogenic aerosols along the Gangetic Plains, which act to warm the mid-troposphere (Lodhi et al. 2013; Wang et al. 2013b; Kastaoutis et al. 2014). Interdecadal climate variations due to natural causes do exist and can affect Nepal (e.g., Guhathakurta et al. 2014; Wang et al. 2013a) and these cannot be ruled out, but, the CMIP5 analysis does paint a probable scenario whereby increasing anthropogenic GHGs and aerosols are envisaged to contribute to change in regional storm tracks. Future work will focus on examining the full archive of CMIP5 model outputs in order to validate and quantify the impact of individual climate forcings.

c. Implication to weather patterns. The collective changes in the upper and lower circulations suggest that the chance for synoptic short waves crossing northern India to interact with BoB TCs intruding into the Gangetic Plains has increased. To clarify this supposition, we derived the daily eddy geopotential height (Z_E) on 13–14 October 2015 and compared it with Z_E of any given day during the September 15–November 15 period in order to identify past synoptic settings similar to October 2014. The comparison was made within the domains of 55°–85°E, 20°–45°N for 250 hPa and 65°–95°E, 5°–35°N for 850 hPa, based

upon the dimension of the upper trough and TC Hudhud. Supplemental Fig. S18.1a shows these domains overlaid with the observed Z_E. Next, the spatial correlation coefficient (ρ) of daily Z_E was computed between 13–14 October 2014 for each day from 1950 to 2014, for both pressure levels. Fifteen criteria of ρ were defined ranging from 0.6 to 0.9 with an increment of 0.02. At either level, each ρ criterion has to be satisfied for two consecutive days in order to depict the evolution of the October 2014 case. We show in Supplemental Fig. S18.1 the case composites produced from three criteria: 0.9 (b), 0.8 (c), and 0.7 (d), with the number of cases indicated for visual comparison. Naturally, higher ρ results in a lower case number and a more compatible weather pattern in both location and magnitude. It is worth noting that, at ρ=0.9, there was not a single case at 850 hPa that matches the 14 October 2015 situation; this coincides with the earlier observation in Fig. 18.1b that Hudhud was the only TC on record whose residual low ever reached Nepal.

The statistics of the identified cases at both pressure levels are displayed in Fig. 18.2: the occurrence of cases identified by each ρ-criterion is plotted as thin color lines while the mean of the 15 ρ-criteria is given as thick black line. To illustrate the long-term change, the 20-year moving average of the mean occurrence is also plotted as thick red line (one-sided). There appears to be a steady and significant increase that doubles the occurrence of upper troughs since the mid-1990s (Fig. 18.2a). The increase

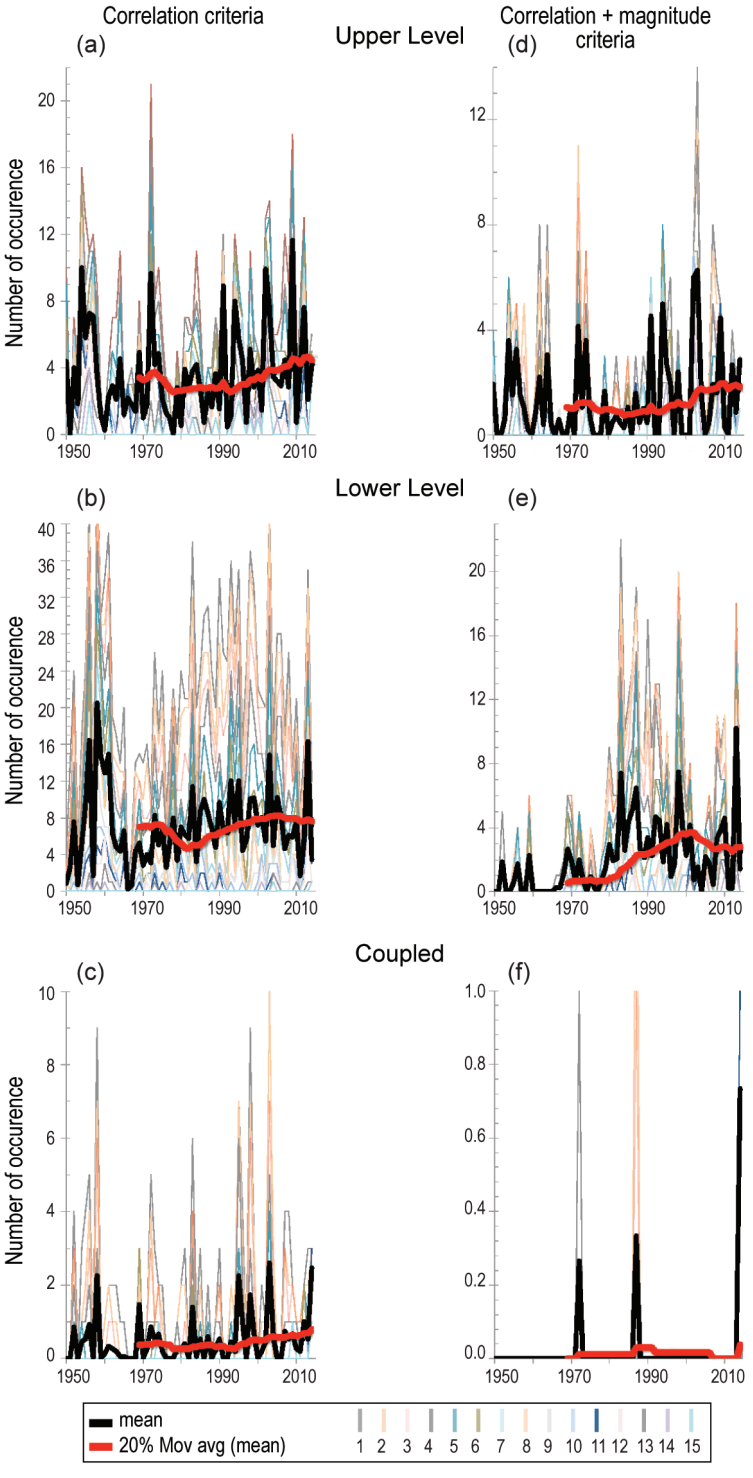

Fig. 18.2. (a) Occurrence of cases identified using the criteria of spatial correlation coefficient (ρ) derived from 250 hPa Z_E, overlaid with the 20-year moving averages (one-sided) . (b) As in (a), but for the 850 hPa level. (c) Same as (a) but for the coupled cases determined by the criteria being met at both levels on the same day. (d)–(f) Similar to (a)–(c) but for the result after the inclusion of RMS on top of the ρ criteria. Notice that some numbers of 2014 exceed the y-axis range.

in the low-level disturbances is also substantial (Fig. 18.2b), though it did not exceed the 1970s high point by much. Next, we introduced an additional criterion for magnitude as determined by the root-mean-square (RMS) of Z_E, which was computed within the domain outlined in Supplemental Fig. S18.1. The RMS has to be at least 80% of that of 13–14 October 2014 at either level. The addition of this magnitude criterion resulted in a reduction in the overall case number, as expected, and it shows a similar range of increase in the upper troughs (Fig. 18.2d). What is more, the magnitude criterion led to a more robust growth of the low-level disturbances after the mid-1980s (Fig. 18.2e), reflecting the intensification of post-monsoon BoB TCs as was discussed earlier.

More importantly, the *concurrence* of the two types of weather systems has indeed increased, as is shown in Fig. 18.2c, determined when the criteria of both levels were met on the same day. The case number of the concurrent weather systems that featured a compatible strength declined substantially (Fig. 18.2f; when taking into account the magnitude criterion), leaving only three years of possible cases including the October 2014 ones. The implication of these results is that, although weather systems similar to that of 13–14 October 2014 did occur in the past, there is a tendency for both types of weather systems to interact more frequently. The potential for heavy precipitation in Nepal as a result of this interaction has increased as well, given the strengthened moisture convergence accompanied by the intensification and northward shift of BoB TCs.

Conclusion. The unusual coupling of a deepened upper trough with the remnants of TC Hudhud over the Nepalese Himalayas enhanced lifting and moisture pooling, causing a blizzard concomitant with heavy snowfall and subsequent avalanches on 14 October 2014. Climate diagnostics point to a tendency for more and/or stronger upper troughs propagating from the Mediterranean region that could coincide with increasingly stronger tropical disturbances coming from BoB. For the lower level, previous studies have linked the intensification of post-monsoon BoB TCs with increased SST and anthropogenic global warming. For the upper level, attribution analyses using an ensemble of 7 CMIP5 models indicate that increased anthropogenic GHG and aerosols both have contributed to the equatorward shift of the jet stream, a feature that arguably diverts more synoptic short waves towards Nepal. By combining these findings, one can conclude that the changing synoptic regimes over both northern India and Nepal would signal an increased possibility of similar events occurring in the future.

ACKNOWLEDGMENT: This study was partly supported by the United States Agency for International Development (USAID) Grant EEM-A-00-10-00001. Comments provided by three anonymous reviewers are highly appreciated.

REFERENCES

Balaguru, K., S. Taraphdar, L. R. Leung, and G. R. Foltz, 2014: Increase in the intensity of postmonsoon Bay of Bengal tropical cyclones. *Geophys. Res. Lett.*, **41**, 3594–3601, doi:10.1002/2014GL060197.

Chen, T.-C., J.-H. Yoon, and S.-Y. Wang, 2005: Westward propagation of the Indian monsoon depression. *Tellus*, **57A**, 758–769.

Gillies, R. R., S.-H. Wang, Y. Sun, and O. Y. Chung, 2013: Supportive empirical modelling for the forecast of monsoon precipitation in Nepal. *Int. J. Climatol.*, **33**, 3047–3054, doi:10.1002/joc.3649.

Guhathakurta, P., M. Rajeevan, D. R. Sikka, and A. Tyagi, 2014: Observed changes in southwest monsoon rainfall over India during 1901–2011. *Int. J. Climatol.*, **35**, 1881–1898, doi:10.1002/joc.4095.

Joyce, R. J., J. E. Janowiak, P. A. Arkin, and P. Xie, 2004: CMORPH: A method that produces global precipitation estimates from passive microwave and infrared data at high spatial and temporal resolution. *J. Hydrometeor.*, **5**, 487–503.

Kalnay, E., and Coauthors, 1996: The NCEP/NCAR 40-year reanalysis project. *Bull. Amer. Meteor. Soc.*, **77**, 437–471.

Kanamitsu, M., W. Ebisuzaki, J. Woollen, S.-K. Yang, J. J. Hnilo, M. Fiorino, and G. L. Potter, 2002: NCEP-DOE AMIP-II Reanalysis (R-2). *Bull. Amer. Meteor. Soc.*, **83**, 1631–1643.

Kaskaoutis, D. G., and Coauthors, 2014: Synoptic weather conditions and aerosol episodes over Indo-Gangetic Plains, India. *Climate Dyn.*, **43**, 2313–2331, doi:10.1007/s00382-014-2055-2.

Kim, J.-S., R. C.-Y. Li, and W. Zhou, 2012: Effects of the Pacific–Japan teleconnection pattern on tropical cyclone activity and extreme precipitation events over the Korean peninsula. *J. Geophys. Res.*, **117**, D18109, doi:10.1029/2012JD017677.

Lau, N.-C., and M. J. Nath, 1991: Variability of the baroclinic and barotropic transient eddy forcing associated with monthly changes in the midlatitude storm tracks. *J. Atmos. Sci.*, **48**, 2589–2613.

Lodhi, N. K., S. N. Beegum, S. Singh, and K. Kumar, 2013: Aerosol climatology at Delhi in the western Indo-Gangetic Plain: Microphysics, long-term trends, and source strengths. *J. Geophys. Res. Atmos.*, **118**, 1361–1375, doi:10.1002/jgrd.50165.

Nair, R. J., and G. Sharma, 2014: Nepal blames poor forecasts, lax rules for trek disaster. Reuters, 17 October, 1:47 p.m. EDT. [Available online at www.reuters.com/article/2014/10/17/uk-nepal-hikers-idUSKCN0I622720141017.]

Rao, S. A., A. R. Dhakate, S. K. Saha, S. Mahapatra, H. S. Chaudhari, S. Pokhrel, and S. K. Sahu, 2012: Why is Indian Ocean warming consistently? *Climatic Change*, **110**, 709–719, doi:10.1007/s10584-011-0121-x.

Riemer, M., and S. C. Jones, 2014: Interaction of a tropical cyclone with a high-amplitude, midlatitude wave pattern: Waviness analysis, trough deformation and track bifurcation. *Quart. J. Roy. Meteor. Soc.*, **140**, 1362–1376, doi:10.1002/qj.2221.

Sahoo, B., and P. K. Bhaskaran, 2015: Assessment on historical cyclone tracks in the Bay of Bengal, east coast of India. *Int. J. Climatol.*, doi:10.1002/joc.4331, in press.

Sarthi, P. P., A. Agrawal, and A. Rana, 2015: Possible future changes in cyclonic storms in the Bay of Bengal, India under warmer climate. *Int. J. Climatol.*, **35**, 1267–1277, doi:10.1002/joc.4053.

Taylor, K. E., R. J. Stouffer, and G. A. Meehl, 2012: An overview of CMIP5 and the experiment design. *Bull. Amer. Meteor. Soc.*, **93**, 485–498, doi:10.1175/BAMS-D-11-00094.1.

Wang, S.-Y., R. E. Davies, W. R. Huang, and R. R. Gillies, 2011: Pakistan's two-stage monsoon and links with the recent climate change. *J. Geophys. Res.*, **116**, D16114, doi:10.1029/2011JD015760.

——, J.-H. Yoon, R. R. Gillies, and C. Cho, 2013a: What caused the winter drought in western Nepal during recent years? *J. Climate*, **26**, 8241–8256, doi:10.1175/JCLI-D-12-00800.1.

——, B. M. Buckley, J. H. Yoon, and B. O. Fosu, 2013b: Intensification of premonsoon tropical cyclones in the Bay of Bengal and its impacts on Myanmar. *J. Geophys. Res. Atmos.*, **118**, 4373–4384, doi:10.1002/jgrd.50396.

Table 34.1. ANTHROPOGENIC INFLUENCE

ON EVENT STRENGTH †

	INCREASE	DECREASE	NOT FOUND OR UNCERTAIN
Heat	**Australia** (Ch. 31) **Europe** (Ch.13) **S. Korea** (Ch. 19)		**Australia, Adelaide & Melbourne** (Ch. 29) **Australia, Brisbane** (Ch.28)
Cold		**Upper Midwest** (Ch.3)	
Winter Storms and Snow			**Eastern U.S.** (Ch. 4) **N. America** (Ch. 6) **N. Atlantic** (Ch. 7)
Heavy Precipitation	**Canada**** (Ch. 5)		**Jakarta****** (Ch. 26) **United Kingdom***** (Ch. 10) **New Zealand** (Ch. 27)
Drought	**E. Africa** (Ch. 16) **E. Africa*** (Ch. 17) **S. Levant** (Ch. 14)		**Middle East and S.W. Asia** (Ch. 15) **N.E. Asia** (Ch. 21) **Singapore** (Ch. 25)
Tropical Cyclones			**Gonzalo** (Ch. 11) **W. Pacific** (Ch. 24)
Wildfires			**California** (Ch. 2)
Sea Surface Temperature	**W. Tropical & N.E. Pacific** (Ch. 20) **N.W. Atlantic & N.E. Pacific** (Ch. 13)		
Sea Level Pressure	**S. Australia** (Ch. 32)		
Sea Ice Extent			**Antarctica** (Ch. 33)

† Papers that did not investigate strength are not listed.

†† Papers that did not investigate likelihood are not listed.

* No influence on the likelihood of low rainfall, but human influences did result in higher temperatures and increased net incoming radiation at the surface over the region most affected by the drought.

** An increase in spring rainfall as well as extensive artificial pond drainage increased the risk of more frequent severe floods from the enhanced rainfall.

*** Evidence for human influence was found for greater risk of UK extreme rainfall during winter 2013/14 with time scales of 10 days

**** The study of Jakarta rainfall event of 2014 found a statistically significant increase in the probability of such rains over the last 115 years, though the study did not establish a cause.

	ON EVENT LIKELIHOOD ††			Total Number of Papers
	INCREASE	DECREASE	NOT FOUND OR UNCERTAIN	
Heat	**Argentina** (Ch. 9) **Australia** (Ch. 30, Ch. 31) **Australia, Adelaide** (Ch. 29) **Australia, Brisbane** (Ch. 28) **Europe** (Ch. 13) **S. Korea** (Ch. 19) **China** (Ch. 22)		**Melbourne, Australia** (Ch. 29)	7
Cold		**Upper Midwest** (Ch.3)		1
Winter Storms and Snow	**Nepal** (Ch. 18)		**Eastern U.S.**(Ch. 4) **N. America** (Ch. 6) **N. Atlantic** (Ch. 7)	4
Heavy Precipitation	**Canada**** (Ch. 5) **New Zealand** (Ch. 27)		**Jakarta****** (Ch. 26) **United Kingdom***** (Ch. 10) **S. France** (Ch. 12)	5
Drought	**E. Africa** (Ch. 16) **S. Levant** (Ch. 14)		**Middle East and S.W. Asia** (Ch. 15) **E. Africa*** (Ch. 17) **N.E. Asia** (Ch. 21) **S. E. Brazil** (Ch. 8) **Singapore** (Ch. 25)	7
Tropical Cyclones	**Hawaii** (Ch. 23)		**Gonzalo** (Ch. 11) **W. Pacific** (Ch. 24)	3
Wildfires	**California** (Ch. 2)			1
Sea Surface Temperature	**W. Tropical & N.E. Pacific** (Ch. 20) **N.W. Atlantic & N.E. Pacific** (Ch. 13)			2
Sea Level Pressure	**S. Australia** (Ch. 32)			1
Sea Ice Extent			**Antarctica** (Ch. 33)	1
			TOTAL	32

† Papers that did not investigate strength are not listed.

†† Papers that did not investigate likelihood are not listed.

* No influence on the likelihood of low rainfall, but human influences did result in higher temperatures and increased net incoming radiation at the surface over the region most affected by the drought.

** An increase in spring rainfall as well as extensive artificial pond drainage increased the risk of more frequent severe floods from the enhanced rainfall.

*** Evidence for human influence was found for greater risk of UK extreme rainfall during winter 2013/14 with time scales of 10 days

**** The study of Jakarta rainfall event of 2014 found a statistically significant increase in the probability of such rains over the last 115 years, though the study did not establish a cause.